Water Penetration through a Superhydrophobic Mesh During a Drop Impact

Seunggeol Ryu,[1] Prosenjit Sen,[2] Youngsuk Nam,[1,*] and Choongyeop Lee[1,†]
[1]Department of Mechanical Engineering, Kyung Hee University, Yongin 17104, Republic of Korea
[2]Center for Nanoscience and Engineering, Indian Institute of Science, Bengaluru, Karnataka 560012, India
(Received 12 September 2016; revised manuscript received 17 November 2016; published 3 January 2017)

When a water drop impacts a mesh having submillimeter pores, a part of the drop penetrates through the mesh if the impact velocity is sufficiently large. Here we show that different surface wettability, i.e., hydrophobicity and superhydrophobicity, leads to different water penetration dynamics on a mesh during drop impact. We show, despite the water repellence of a superhydrophobic surface, that water can penetrate a superhydrophobic mesh more easily (i.e., at a lower impact velocity) over a hydrophobic mesh via a penetration mechanism unique to a superhydrophobic mesh. On a superhydrophobic mesh, the water penetration can occur during the drop recoil stage, which appears at a lower impact velocity than the critical impact velocity for water penetration right upon impact. We propose that this unique water penetration on a superhydrophobic mesh can be attributed to the combination of the hydrodynamic focusing and the momentum transfer from the water drop when it is about to bounce off the surface, at which point the water drop retrieves most of its kinetic energy due to the negligible friction on superhydrophobic surfaces.

DOI: 10.1103/PhysRevLett.118.014501

With reduced interaction with water [1], superhydrophobic (SHPo) surfaces can be used for frictional drag reduction [2–4], water harvesting [5,6], self-cleaning [7], anti-icing [8], antifouling [9], and heat transfer enhancement [10,11]. Particularly, a mesh-type SHPo surface having a preexisting array of pores with diameters in the tens to hundreds of micrometer range can be used as a fluid sieve to selectively capture or separate one fluid phase from another, e.g., water moisture from fog (i.e., an air-water mixture) [12], gas bubbles from a two-phase stream [13], and water from an oil-water mixture [14]. In such examples, it has been shown that the surface wettability has a significant influence on the sieving performance of a mesh. Also, a mesh can be an ideal starting material to fabricate a multiscale SHPo surface due to its preexisting pores, as multiscale structures can exhibit more robust superhydrophobicity against external disturbances compared with single-scale ones [15,16].

On SHPo surfaces, of particular interest is their interaction with impacting water drops, as a drop impact is a frequently encountered physical event in many industrial processes such as cooling, combustion, inkjet printing, and surface coating [17,18]. When an impact velocity is moderately small, the SHPo mesh can effectively repel the incoming drops. However, if the impact velocity of a water drop is sufficiently large, the water drop can penetrate through the mesh, which might compromise the performance of the SHPo mesh for certain applications, where the water penetration is undesirable.

Previous studies investigated water penetration through a single pore or a porous mesh or membrane during drop impact to understand the influence of pore geometry [19,20] and surface wettability [21,22] on the required impact velocity for water penetration. It has been shown that the penetration is determined by a balance between the dynamic pressure of a water drop and the capillarity (or Laplace pressure) [19,20]. Also, a nonwettable multiscale SHPo or single-scale hydrophobic (HPo) mesh has been tested to determine the influence of hydrophobicity on the penetration behavior. While one study showed that there was no distinctive influence of surface wettability [21], other studies claimed the better resistance of nonwettable SHPo mesh against water penetration over a hydrophilic (HPi) [22,23] and HPo mesh [23].

However, contrary to those previous results, we show that water can penetrate more easily through the SHPo mesh over the HPo mesh with the emergence of an additional penetration mechanism on the SHPo mesh, which occurs during recoil and at a lower impact velocity than the required velocity for the penetration right upon impact.

Experimental method.—In the present study, the Cu mesh (>99% purity, TWP Inc.) with a well-defined pore geometry was used after surface treatment (hydrophobicity or superhydrophobicity), as reported in Ref. [24] and detailed in the Supplemental Material [25]. The scanning electron microscopy image of the modified SHPo mesh is shown in Fig. 1 along with the geometric information of the tested meshes. To capture the penetration dynamics of the impacting drop through a mesh, a water drop of the given diameter (2.5 mm) was released from the known height, and the impact and penetration dynamics was captured using a high-speed camera (Phantom M110) at up to 9500 frames/sec.

Results.—We observed from the captured images a noticeable difference in the penetration behavior between

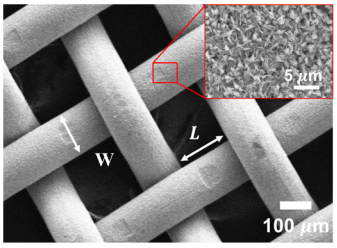

Mesh number	W [μm]	L [μm]
200	52	72
145	55.9	101.6
100	114.3	139.7
80	139.7	177.8
60	190.5	228.6
50	228.6	279.4
40	254.0	381.0

FIG. 1. Scanning electron microscopy images of superhydrophobic mesh along with geometric details of the tested mesh in the present study.

the HPo mesh and SHPo mesh. Figure 2 shows sequential images of the penetration dynamics on the HPo mesh [Fig. 2(a)] and SHPo mesh [Fig. 2(b)], respectively. At a low impact velocity, no penetration is observed both on the HPo mesh and SHPo mesh (Videos S1 and S2 in Ref. [25]). However, when the impact velocity is increased, the penetration first appears on the SHPo mesh (Video S4 in Ref. [25]), while there is still no water penetration on the HPo mesh (Video S3 in Ref. [25]). Interestingly, the penetration does not occur right upon impact as generally thought, but it occurs during drop recoil. With a further increase of the impact velocity, the penetration upon impact is observed both on the HPo mesh and SHPo mesh but with a clear difference (Videos S5 and S6 in Ref. [25]). On the SHPo mesh, the penetrated water completely detaches from the main drop [i.e., "complete penetration" (C)], while on the HPo mesh, it fails to detach from the main drop, resulting in the incomplete penetration [i.e., "incomplete penetration" (I)]. Only when the impact velocity is sufficiently large, the water completely penetrates through the HPo mesh (Video S7 in Ref. [25]). Also, on the SHPo mesh, the water penetration during recoil persists even after the emergence of the water penetration upon impact, and the penetration velocity during recoil is faster than the penetration velocity during impact (Video S8 in Ref. [25]).

Generally, the penetration dynamics through a mesh can be explained based on the force balance between the penetration pressure and the resisting capillary force, which can be written as $\Delta PA > \gamma\Gamma$ [20,26,27]. Here, A and Γ represent the opening area ($\approx L^2$) and perimeter ($\approx 4L$) of a single pore, respectively, and γ is the surface tension of water (72 mN/m). Accordingly, $\gamma\Gamma/A$ will be the capillary antipenetration pressure, which needs to be overcome for the water penetration through a mesh to occur; i.e., only when the penetration pressure (ΔP) is larger than this antipenetration pressure ($\gamma\Gamma/A$) will the water penetrate through the mesh. In Fig. 3, the penetration diagrams are plotted as a function of this capillary antipenetration pressure and impact velocity for the HPo [Fig. 3(a)] and SHPo [Fig. 3(b)] meshes, respectively. Here, to differentiate each penetration case in the simplistic way, we categorized the penetration behaviors based on its timing [i.e., "IP" (impact penetration) and "RP" (recoil penetration)] and its extent [i.e., "N" (no penetration), "I" (incomplete penetration), and "C" (complete penetration)].

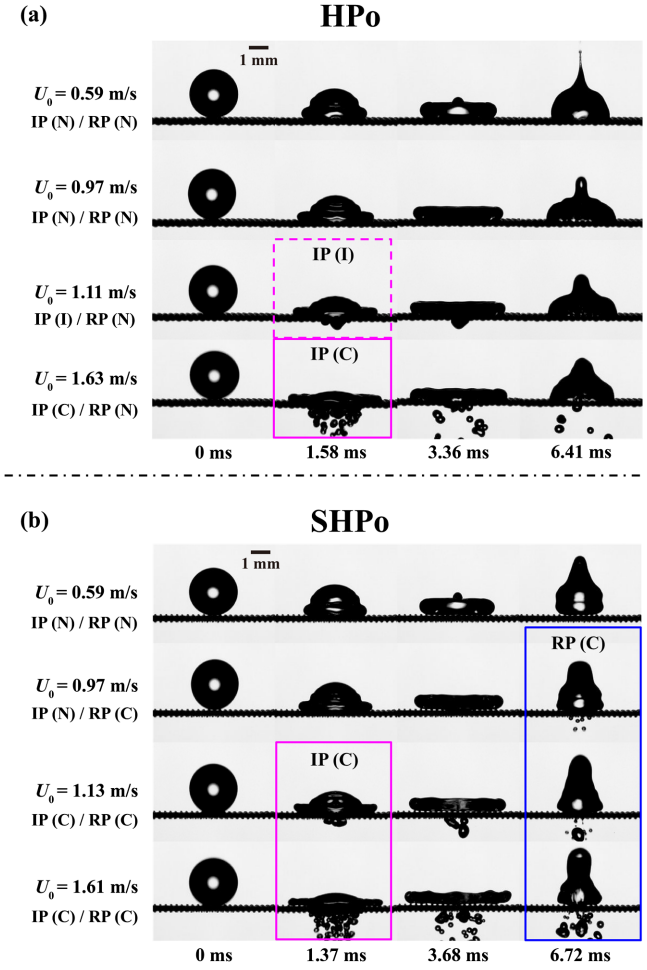

FIG. 2. Sequential images of drop impact dynamics as a function of the impact velocity on (a) hydrophobic and (b) superhydrophobic meshes (mesh no. 100).

In Fig. 3(a), it can be seen that when the impact velocity is increased on the HPo meshes, two types of penetration transitions, i.e., first the transition from IP(N) to IP(I) and then the transition from IP(I) to IP(C), are universally observed, while there is no RP on all tested HPo meshes. On the other hand, the penetration diagram on the SHPo mesh in Fig. 3(b) appears more complicated due to the presence of RP. Generally, on the SHPo mesh, RP appears at a lower impact velocity than IP, but the difference between the two critical impact velocities for IP and RP decreases when the opening size becomes larger (or $\gamma\Gamma/A$ becomes smaller), implying that IP and RP follow different velocity dependence. Also, although the incomplete penetration is a rarer event on the SHPo mesh compared with the HPo mesh, it tends to occur more frequently as the opening size becomes larger.

Please note that in SHPo meshes with a large pore size (i.e., $L > 230$ μm), we observed the absence of RP at the relatively large impact velocity, which is attributed to the

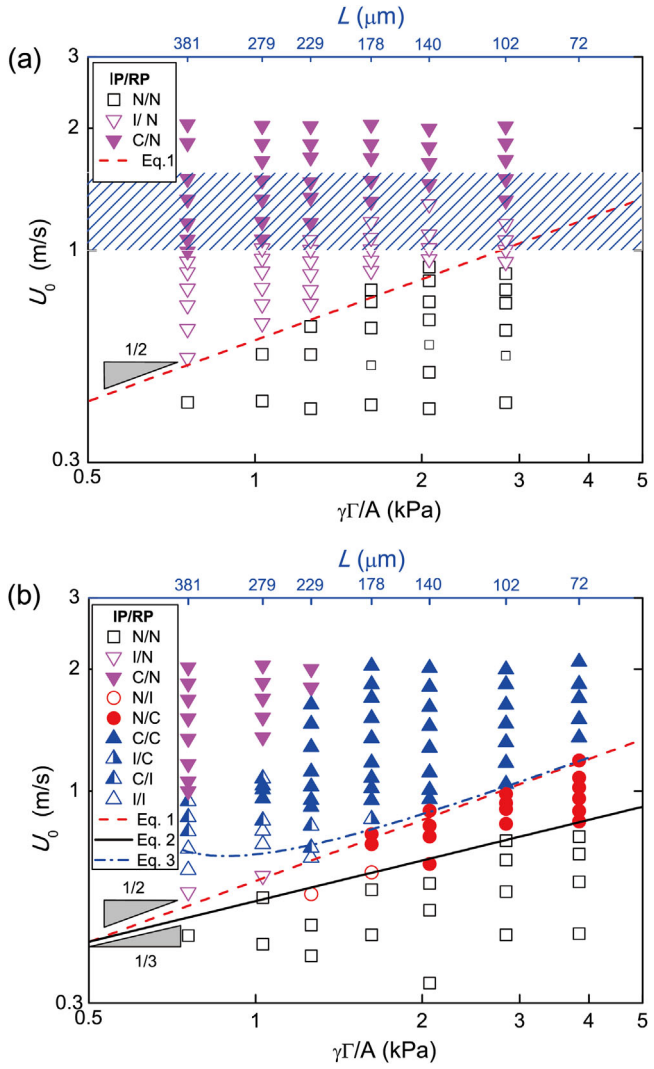

FIG. 3. Penetration diagram in log-log scale as a function of the impact velocity and the capillary antipenetration pressure on (a) hydrophobic and (b) superhydrophobic meshes.

early bouncing of the water drop from the mesh after impact (Video S9 in Ref. [25]). However, this specific case is not a focus of the present study, as the mechanism of an early bouncing behavior has already been elucidated in recent studies [28,29], and it involves a different physical mechanism from other penetration behaviors.

One can explain the water penetration pressure ΔP using the momentum transfer upon impact, as shown in Fig. 4. When the momentum M is delivered upon the surface area A_c over a time scale τ, it results in the penetration pressure $\Delta P \sim M/(A_c\tau)$.

Right upon an impact, the water drop imparts $M \sim \rho D_0^3 U_0$ upon $A_c \sim D_0^2$, over $\tau \sim D_0/U_0$ (i.e., the deceleration time of the water drop), resulting in the penetration pressure $\Delta P \sim \rho U_0^2$ (i.e., a dynamic pressure) [30]. When this dynamic pressure is equated with the antipenetration pressure acting on each pore, one obtains

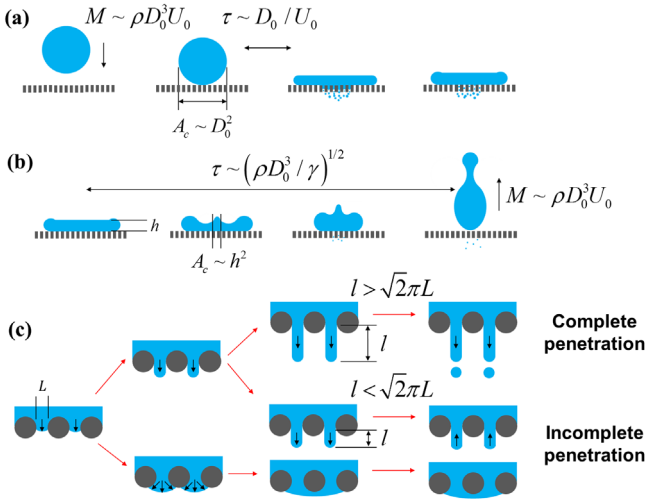

FIG. 4. Schematics for the origin of the penetration pressures (a) right upon impact and (b) during recoil. (c) Possible physical mechanisms responsible for complete penetration and incomplete penetration.

$C_0\rho U_0^2 = \gamma\Gamma/A$ with C_0 being a proportionality constant. From this relationship, we obtain the critical penetration velocity upon impact, which is given by the following relationship [26]:

$$U_{c,\mathrm{IP}} \sim \sqrt{1/\rho}\sqrt{\gamma\Gamma/A}. \quad (1)$$

Figures 3(a) and 3(b) show that Eq. (1) [a red dotted line ($C_0 = 2.78$)] well predicts the critical velocity $U_{c,\mathrm{IP}}$ for IP [i.e., the transition from IP(N) to either IP(I) or IP(C)], which follows the $1/2$ power of $\gamma\Gamma/A$. Here, C_0 is about 1.6 times the reported value in the previous study [31], and the discrepancy between the two values might be attributed to a nonplanar 3D geometry of the actual mesh pore, while the analysis is based on the planar and square pore shape.

During recoil of the water drop on the SHPo mesh in Fig. 2(b), one can see that the occurrence of RP corresponds to the instant when the bulge in the central part (i.e., Worthington jet) of a water drop is moving upwards. Then, the penetration pressure during recoil may be attributed to the momentum transfer onto the surface during takeoff of the water. A previous study shows that after impact over the SHPo surface, the water drop retrieves most of its initial kinetic energy due to the negligible frictional dissipation [32]. Meanwhile, on the HPo mesh, there is a greater amount of frictional dissipation, and, thus, the water drop fails to bounce off the HPo mesh. Then, on the SHPo mesh, during takeoff, the water drop will impart a momentum, which is comparable with the initial momentum before impact $M \sim \rho D_0^3 U_0$, and the relevant time scale will be determined by the balance between inertia ($\sim \rho D_0^3 D_{\max}/\tau^2$) and surface tension ($\sim \gamma D_{\max}$) during retraction, which is the Rayleigh oscillation time $\tau \sim (\rho D_0^3/\gamma)^{1/2}$ [33]. Lastly, one can assume that the penetration diameter during recoil

is comparable to the jet diameter, which is, in turn, scaled with the film thickness h at the maximal deformation, as shown in Fig. 4(b) (i.e., $A_c \sim h^2$). As the film thickness h is scaled as $h \sim \sqrt{\gamma/\rho(U_0^2/D_0)}$ [34], one obtains $A_c \sim \rho^{-1} D_0 U_0^{-2} \gamma$. Please note that the scaling $A_c \sim U_0^{-2}$ was indeed confirmed on the SHPo surface in the velocity range where RP was observed (Fig. S1 in Ref. [25]). Then, the penetration pressure during recoil will be scaled as $\Delta P \sim M/(A_c \tau) \sim \rho^{3/2} D_0^{1/2} U_0^3 \gamma^{-1/2}$. Equating it to the antipenetration pressure ($\Delta P = C_1 \rho^{3/2} D_0^{1/2} U_0^3 \gamma^{-1/2} = \gamma\Gamma/A$) yields the following relation:

$$U_{c,\mathrm{RP}} \sim \rho^{-1/2} D_0^{-1/6} \gamma^{1/6} (\gamma\Gamma/A)^{1/3}. \quad (2)$$

In Fig. 3(b), Eq. (2) [the black solid line ($C_1 = 0.0384$)] exhibits good agreement with the experimental data such that the critical velocity $U_{c,\mathrm{RP}}$ for RP indeed follows the $1/3$ power of $\gamma\Gamma/A$. Additionally, Eq. (2) predicts weak dependence of the critical velocity on the drop diameter $U_{c,\mathrm{RP}} \sim D_0^{-1/6}$ for RP, in line with our observation that $U_{c,\mathrm{RP}}$ does not vary much when D_0 ranges between 2.2 and 3.3 mm (Fig. S2 in Ref. [25]).

A comparison of Eqs. (1) and (2) suggests that the presence of RP can be attributed to the hydrodynamic focusing of a special kind. During recoil, it is expected that the momentum M decreases over the initial value even on the SHPo mesh, while the time scale τ for the momentum transfer during recoil is normally larger than that upon impact, both of which contribute towards the decrease of penetration pressure during recoil. However, the momentum transfer is focused on a much smaller area A_c during recoil, compensating other factors and leading to the larger penetration pressure during recoil compared with the pressure upon impact. As a result, despite its water repellency, the SHPo surface can make a mesh more vulnerable to the penetration over the HPo mesh.

Back to the IP, the presence of IP(I) in between IP(N) and IP(C) may be explained based on the Rayleigh-Plateau instability theory [19,35]. When a diameter of cylindrical water jet is d, the most amplified wavelength, i.e., the required transverse length for a pinch-off, is given by $\sqrt{2}\pi d$ [19,35]. During penetration through the mesh, there will be the pressure drop by the antipenetration pressure $\sim \rho U_{c,\mathrm{IP}}^2$, resulting in the water velocity $U_0\sqrt{1-(U_{c,\mathrm{IP}}/U_0)^2}$ after penetration. Using D_0/U_0 as the characteristic time during IP and the opening size ($d = L$) as the jet diameter, the criteria for the complete penetration are expressed as

$$\sqrt{1-(U_{c,\mathrm{IP}}/U_0)^2} > \sqrt{2}\pi(d/D_0). \quad (3)$$

Equation (3) is plotted in Fig. 3(b) as the blue dash-dot line without any fitting parameter, and it well captures the IP(I) regime as a function of the opening size L (or antipenetration pressure) on the SHPo mesh. Particularly, Eq. (3) shows that decreasing a pore size (i.e., increasing the antipenetration pressure) does not always lead to the enhanced resistance against IP(C), as the transition IP(I) to IP(C) is more favorable on a smaller pore size.

However, Eq. (3) cannot explain the IP(I) regime on the HPo mesh, and the main reason may lie in the difference of the actual jet diameter d after penetration on the HPo and SHPo meshes. After penetration, the water out of each opening may flow along the mesh surface and merge with adjacent ones [Fig. 4(c)]. If this is the case, the effective jet diameter d will be much larger than the pore size L, resulting in an increase in the required transverse length for a pinch-off. For example, Eq. (3) implies that if the jet diameter d is much larger than a pore size L and is comparable to the drop diameter (such as $d/D_0 > 0.225$), IP(C) is unlikely to occur. According to a previous study [36], whether water flows along the surface having a high curvature was strongly dependent on the surface wettability and the flow velocity such that the separation of the water flow occurred over the SHPo surface at all test flow velocities, while the required minimum velocity for flow separation on the HPo surface was about 1–1.5 m/s, which is comparable with the critical velocity for the transition from IP(I) to IP(C) in the present study [shaded in blue in Fig. 3(a)]. It means that the transition from IP(I) to IP(C) on the HPo mesh may be the direct consequence of progressively nonmerging behaviors of several adjacent water flows after penetration, as the water flow is separated from the HPo surface due to the increased inertia.

In summary, the drop impact on the SHPo mesh can lead to two penetration mechanisms, i.e., upon impact (IP) and during recoil (RP). While IP is common to both the HPo mesh and the SHPo mesh, RP is unique to the SHPo mesh, as a negligible frictional dissipation on the SHPo mesh is a prerequisite for RP, and the presence of RP makes the SHPo mesh more vulnerable to the water penetration during impact compared with the HPo mesh.

This work was supported by the Basic Science Research Program (Grants No. 2015R1A1A1A05001412 and No. 2014R1A1A1002908), the International Cooperation Program in Science and Technology (Grant No. 2014K1A3A1A19066962), and the Fundamental Technology Research Program (Grant No. 2014M3A7B4052202) through the National Research Foundation of Korea funded by the Ministry of Science, ICT and Future Planning.

*ysnam1@khu.ac.kr
†cylee@khu.ac.kr

[1] D. Quéré, Rep. Prog. Phys. **68**, 2495 (2005).
[2] C. Lee, C.-H. Choi, and C.-J. Kim, Phys. Rev. Lett. **101**, 064501 (2008).
[3] C. Lee and C.-J. Kim, Langmuir **25**, 12812 (2009).
[4] C. Lee and C.-J. Kim, Langmuir **27**, 4243 (2011).

[5] D. Seo, C. Lee, and Y. Nam, Langmuir **30**, 15468 (2014).
[6] D. Seo, J. Lee, C. Lee, and Y. Nam, Sci. Rep. **6**, 24276 (2016).
[7] W. Barthlott and C. Neinhuis, Planta **202**, 1 (1997).
[8] M. J. Kreder, J. Alvarenga, P. Kim, and J. Aizenberg, Nat. Rev. Mater. **1**, 15003 (2016).
[9] G. D. Bixler and B. Bhushan, Phil. Trans. R. Soc. A **370**, 2381 (2012).
[10] N. Miljkovic, R. Enright, Y. Nam, K. Lopez, N. Dou, J. Sack, and E. N. Wang, Nano Lett. **13**, 179 (2013).
[11] H. Kim and Y. Nam, Int. J. Heat Mass Transfer **93**, 286 (2016).
[12] K.-C. Park, S. S. Chhatre, S. Srinivasan, R. E. Cohen, and G. H. McKinley, Langmuir **29**, 13269 (2013).
[13] X. Hou, Y. Hu, A. Grinthal, M. Khan, and J. Aizenberg, Nature (London) **519**, 70 (2015).
[14] A. K. Kota, G. Kwon, W. Choi, J. M. Mabry, and A. Tuteja, Nat. Commun. **3**, 1025 (2012).
[15] M. McCarthy, K. Gerasopoulos, R. Enright, J. N. Culver, R. Ghodssi, and E. N. Wang, Appl. Phys. Lett. **100**, 263701 (2012).
[16] M. Nosonovsky, Langmuir **23**, 3157 (2007).
[17] A. Yarin, Annu. Rev. Fluid Mech. **38**, 159 (2006).
[18] C. Josserand and S. Thoroddsen, Annu. Rev. Fluid Mech. **48**, 365 (2016).
[19] P. Brunet, F. Lapierre, F. Zoueshtiagh, V. Thomy, and A. Merlen, Appl. Phys. Lett. **95**, 254102 (2009).
[20] É. Lorenceau and D. Quéré, J. Colloid Interface Sci. **263**, 244 (2003).
[21] R. P. Sahu, S. Sinha-Ray, A. L. Yarin, and B. Pourdeyhimi, Soft Matter **8**, 3957 (2012).
[22] R. Sahu, S. Sett, A. Yarin, and B. Pourdeyhimi, Colloids Surf. A **467**, 31 (2015).
[23] T. An, S. J. Cho, W. Choi, J. H. Kim, S. T. Lim, and G. Lim, Soft Matter **7**, 9867 (2011).
[24] Y. Nam and Y. S. Ju, J. Adhes. Sci. Technol. **27**, 2163 (2013).
[25] See the Supplemental Material at http://link.aps.org/supplemental/10.1103/PhysRevLett.118.014501 for the fabrication details and videos.
[26] C. Lee, Y. Nam, H. Lastakowski, J. I. Hur, S. Shin, A.-L. Biance, C. Pirat, C.-J. Kim, and C. Ybert, Soft Matter **11**, 4592 (2015).
[27] D. Bartolo, F. Bouamrirene, É. Verneuil, A. Buguin, P. Silberzan, and S. Moulinet, Europhys. Lett. **74**, 299 (2006).
[28] A. Gauthier, S. Symon, C. Clanet, and D. Quéré, Nat. Commun. **6**, 8001 (2015).
[29] J. C. Bird, R. Dhiman, H.-M. Kwon, and K. K. Varanasi, Nature (London) **503**, 385 (2013).
[30] D. Soto, A. B. De Lariviere, X. Boutillon, C. Clanet, and D. Quéré, Soft Matter **10**, 4929 (2014).
[31] I. V. Roisman, E. Berberović, and C. Tropea, Phys. Fluids **21**, 052103 (2009).
[32] A.-L. Biance, F. Chevy, C. Clanet, G. Lagubeau, and D. Quéré, J. Fluid Mech. **554**, 47 (2006).
[33] D. Richard, C. Clanet, and D. Quéré, Nature (London) **417**, 811 (2002).
[34] C. Clanet, C. Béguin, D. Richard, and D. Quéré, J. Fluid Mech. **517**, 199 (2004).
[35] J. Eggers, Rev. Mod. Phys. **69**, 865 (1997).
[36] C. Duez, C. Ybert, C. Clanet, and L. Bocquet, Phys. Rev. Lett. **104**, 084503 (2010).